Excitation energy division in the quasielastic region from reactions of 12 MeV/nucleon ^{48}Ti with ^{150}Nd

T. M. Semkow, D. G. Sarantites, K. Honkanen,* Z. Li,† and M. Ross
Department of Chemistry, Washington University, St. Louis, Missouri 63130

J. R. Beene, M. L. Halbert, and D. C. Hensley
Oak Ridge National Laboratory, Oak Ridge, Tennessee 37831
(Received 20 January 1987; revised manuscript received 20 August 1987)

Internal excitation of projectile-like fragments and target-like fragments was investigated for the system 12 MeV/nucleon ^{48}Ti + ^{150}Nd, by measuring the discrete γ rays emitted by both fragments in coincidence with the charge-separated projectile-like fragments. Two quasielastic exit channels of the projectile-like fragments were studied: $Z=20$ and $Z=22$. Characteristic γ rays were used to determine the average masses of products, after separation and neutron evaporation, as a function of kinetic energy loss. Our results show that the mass-to-charge equilibration occurs quickly for the $Z=20$ exit channel, but is slower for the $Z=22$ channel. Comparison between the average masses of products with the masses calculated using the statistical model show that the excitation energy is divided approximately equally between the projectile-like and the target-like fragments for the $Z=20$ exit channel. The excitation energy appears to be divided equally up to $\sim$105 MeV of the kinetic energy loss corresponding to $\sim$36% of kinetic energy damping. This result is consistent with predictions made by the stochastic nucleon-exchange models for a small kinetic energy loss.

I. INTRODUCTION

Reactions between two colliding heavy ions leading to the formation of dinuclear systems have been studied extensively in recent years in low and medium energy nuclear physics. The dinuclear system in the entrance channel maintains its binary character during the reaction and two primary fragments leave the interaction zone. The dinuclear systems are formed temporarily in quasielastic and deep inelastic heavy ion collisions (as well as the late stages of the fission process). A review article on the dynamics of dinuclear reactions has been published by Randrup.[1] The relevant aspects of the dynamics of dinucleus are the distribution of mass, charge, excitation energy, and angular momentum between the projectile-like fragments (PLF) and target-like fragments (TLF). In particular, study of the division of excitation energy between two fragments, as a function of the kinetic energy loss ($E_{\rm loss}$), can bring some insight on statistical equilibrium between fragments and possible mechanisms of energy dissipation into internal excitation (heat). The excitation energy acquired by the fragments is removed by evaporating light charged particles, neutrons, and emitting γ rays. Light projectiles may deexcite by sequential particle emission often referred to as a projectile breakup.[2]

Early experiments on deeply inelastic collisions which addressed the subject of excitation energy division utilized measurement of coincidences between PLF and TLF,[3] measurements of neutron multiplicities[4–7] and measurement of energy, time of flight, and specific ionization of the fragments.[8] The conclusions reached were that both fragments for large $E_{\rm loss}$ were in thermal equilibrium, i.e., had the same temperature, which implied that the excitation energy was divided in proportion to the masses (excitation energy is related to the temperature through the Fermi-gas model relation $E^* \propto AT^2$). However, Huizenga *et al.* have pointed out,[9] using an argument of excitation-energy widths, that the temperatures of the two fragments may be different for small $E_{\rm loss}$ in the system 8.3 MeV/nucleon ^{56}Fe + ^{165}Ho. A recent study of the reaction 15.3 MeV/nucleon ^{58}Ni + ^{197}Au by Awes *et al.*[10] indicated that the excitation energy is shared equally between PLF and TLF. Also, a detailed interpretation of ^{56}Fe + ^{165}Ho data shows a near equal energy division for small $E_{\rm loss}$ and a transition to equilibrium energy sharing in the vicinity of full damping ($E_{\rm loss} \sim 160$ MeV).[10,11] Several other experiments have been done on this subject, utilizing a variety of techniques such as fission-product yield distributions,[12,13] measurements of energy spectra of mass and charge separated PLF,[14,15] coincidence measurements of both PLF and TLF with TLF discrete γ rays,[16] PLF in coincidence with their own γ rays,[17,18] coincidences between PLF and light charged particles,[19–21] and coincident measurement of both PLF and TLF.[22] These experiments not only show nonequilibrium energy division, but also that the division depends on the entrance/exit-channel.

Several theoretical models have been developed which deal with the subject of excitation energy division. One group of models is based on stochastic exchange of nucleons between two fragments before separation.[23–26] These models predict a higher temperature of the lighter

partner, as well as an excitation energy division close to equal for low E_{loss}. A transition to equilibrium energy division for higher E_{loss} is expected due to mass and energy flow caused by the temperature gradient. Another model for the excitation energy division utilizes a prescription for calculating the optimum Q value, Q_{opt}.[27] Then the total excitation energy can be calculated as $Q_{gg}-Q_{opt}$ and scaled according to the number of nucleons transferred.[20] This procedure leaves the acceptor hot and the donor cold. In other words, most of the excitation energy is carried away by the PLF for pickup reactions and by the TLF for stripping reactions.

In this experiment we studied the excitation energy division for the reaction ^{48}Ti + ^{150}Nd at $E/A=12$ MeV. We measured characteristic γ rays from both the PLF and TLF in coincidence with the PLF. Also, the total γ energy and multiplicity were measured. Two groups of quasielastic exit channels were studied in detail: $Z=20$ and 22 of the PLF. The intensities of discrete γ rays from Ca/Sm and Ti/Nd products were used to determine the centroids of secondary mass distributions as a function of E_{loss}. A similar technique was used by Sobotka *et al.*[16] with respect to TLF only. The E_{loss} was calculated event-by-event from two-body kinematics, followed by calculation of the total excitation energy, E^*_{tot}. For the $Z=20$ exit channel we were able to deduce the average primary masses of the two outgoing fragments. These masses had the values close to the charge-equilibrated masses, indicating that the charge equilibration occurs quickly for this exit channel. That allowed us to believe that the average primary masses do not shift significantly with E_{loss}. Consequently, comparisons of the functions of mass centroids versus the E^*_{tot} for complementary products (i.e., Ca and Sm) with the statistical-model calculations allowed to estimate that the excitation energy is shared approximately equally between the PLF and TLF. This result holds in the range of $E_{loss}=0-105$ MeV corresponding to a maximum of 36% energy damping. On the contrary, the $Z=22$ exit channel does not show a fast mass-to-charge equilibration, which precluded us from making a determination of the energy sharing in this case.

II. EXPERIMENTAL PROCEDURES

The experiment was performed at the Holifield Heavy-Ion Research Facility using the tandem heavy-ion accelerator in a coupled mode with the ORIC cyclotron. A 1.14 mg/cm^2 thick ^{150}Nd target was bombarded with 581 MeV ^{48}Ti ions. Projectile-like fragments and light ions were detected in four $\Delta E/E$ silicon telescopes positioned at $\theta=20°$ ($\theta_{gr}\cong 17°$), each subtending a solid angle of about 8 msr. The thicknesses of the ΔE detectors varied between 37 and 51 μm, while those of the E detectors ranged from 1500 to 2000 μm. The telescopes had collimators covered with 0.90 mg/cm^2 Ni foils. The target and the telescopes were placed in the spherical scattering chamber inside the spin spectrometer. The spin spectrometer consists of an array of 72 NaI detectors in a 4π geometry.[28] The purpose of the spin spectrometer was to measure total energy of γ rays emitted during the reaction. The beam was stopped in a Faraday cup outside the spin spectrometer. Six NaI elements from the spin spectrometer were replaced with Ge detectors having NaI Compton suppressors positioned; four at $\theta=63°$ and two at 116°. The overall suppression factor was 2.8 for a ^{60}Co source. The Ge detectors were used to detect discrete γ rays from the PLF and TLF. All the forward elements of the spin spectrometer had stacks of Ta, Cd, and Cu plates to absorb the protons, and the Ge detectors had Cu and Cd absorbers for X-ray absorption. Coincident events between any of the $\Delta E/E$ telescopes and at least one Compton-suppressed Ge were accepted as the event trigger. For each accepted event all the other telescopes and Ge (even unsuppressed) were recorded, if fired. In addition, the digitized timing signals from the silicon E and the Ge detectors together with the digitized linear and timing signals from the spin spectrometer were recorded for each event. A software window was placed during data collection to reject most events triggered by α particles and protons, unless in coincidence with heavier PLF.

The spin spectrometer detectors were calibrated with ^{75}Se, ^{207}Bi, ^{88}Y, ^{60}Co, ^{24}Na, and Pu/Be γ-ray sources using established methods.[28] The γ rays in the reaction data from the spin spectrometer were separated from the neutrons by their times of flight.[28] The silicon telescopes were calibrated using a mixed α source (^{233}U, ^{239}Pu, ^{241}Am, ^{244}Cm) and a pulser. In addition, the position of the elastic peak of ^{48}Ti scattered on ^{150}Nd was used in the calibration (the spin spectrometer was used as a filter to select primarily the elastic scattering by accepting such events in which none of the NaI elements fired). Combining the elastic peak position and the reaction kinematics allowed us to correct for the pulse height defect of the Si detectors. Using both the position and intensity of the elastic peak in conjunction with the calculated Rutherford cross section, we were able to determine that the beam was not exactly centered and, consequently, the effective angles of telescopes were different (i.e., $\theta=17.9°$, 18.0°, 22.0°, and 22.2°). The particle data were corrected for gain shifts due to radiation damage, which were changing with time. The calibrated and corrected $(E,\Delta E)$ maps were converted to maps of E(total) versus Z. A sufficient Z resolution up to $Z=23$ was obtained and the mass resolution of isotopes up to $Z\sim 11$ was retained with this procedure. The Ge detectors were calibrated with ^{152}Eu and ^{182}Ta sources and corrected for gain shifts. After all the above instrumental responses were removed the clean data contained over 13 million events.

III. RESULTS

In this section we shall discuss experimental information obtained from each class of detectors. The PLF spectra measured with the Si telescopes will be briefly covered. A more comprehensive description of the discrete γ-ray spectra will be given with a discussion of the Doppler-shift correction. Subsequently, we shall describe how the E_{loss} and E^*_{tot} was calculated and how the mass distributions of various isotopes were deduced as a

function of the E^*_{tot}. The conclusions about mass-to-charge equilibration, and the excitation energy division based on a comparison between the experiment and the statistical-model calculations will be given in Sec. IV.

The E(total) versus Z maps from the Si telescopes showed two distinct components: a quasielastic component for $Z=19-23$ and a deeply inelastic component for $Z=3-23$. The kinetic energy spectra of Ca and Ti PLF detected with a telescope at $\theta=22°$ are shown in Fig. 1. The Ca energy spectrum has a quasielastic peak at $\sim$490 MeV and a deep inelastic component at $\sim$230 MeV, which is cut off due to complete stopping of low energy PLF's in a relatively thick ΔE detector. The high intensity peak at $\sim$540 MeV for the Ti spectrum is due to inelastic scattering, neutron transfer, and evaporation, while the bump on the left of the peak corresponds largely to the neutron transfer and evaporation. The deep inelastic component at $\sim$250 MeV is much weaker.

The γ-ray spectra measured with the Ge detectors had sufficient statistics for identification of both PLF and TLF in the quasielastic region ($Z=20-22$). These γ rays may be subjected to Doppler shifts depending on the source velocity. The γ-ray spectra from the TLF will be discussed first. The TLF partners of PLF detected at forward angles in the quasielastic region move with $v/c \cong 0.015$ and are directed at $\theta \sim 70°$. Due to this fact the effective target thickness increases to about 3.3 mg/cm^2 and all the TLF essentially stop in the target. Since the transition lifetimes for low lying levels in this region (Nd, Pm, and Sm isotopes) are typically of the order of several ps and sometimes fractions of ns, it follows that the TLF come to the rest before emitting γ radiations and, consequently, there is no Doppler shift. The γ-ray spectra of TLF in coincidence with Ca and Ti are shown in Figs. 2(a) and (b), respectively, for a wide E^*_{tot} gate. As shown in Fig. 2(a), several Sm isotopes are observed (in the $A=152-146$ range) corresponding to neutron transfer and evaporation. Figure 2(b) shows several Nd isotopes present ($A=151-144$).

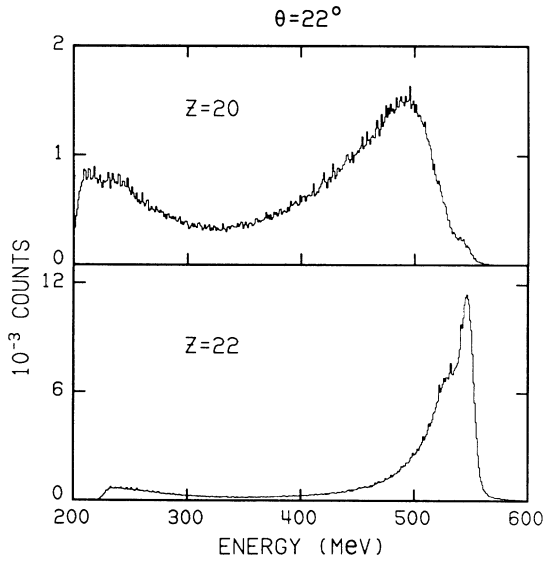

FIG. 1. Kinetic energy spectra of Ca and Ti measured with the $\Delta E/E$ telescope located at $\theta=22°$.

In contrast, the PLF move with high velocities (v/c up to 0.15) in the forward direction. Since they γ decay in flight after leaving the target, Doppler correction is necessary. The Doppler correction was made on an event-by-event basis using standard formulas.[29] The PLF velocities were calculated from two-body kinematics described later. The solid angle ($d\Omega_\gamma^{lab}/d\Omega_\gamma$) correction was also applied,[30] as well as a (small) correction for the PLF energy loss in the target. The same γ-ray spectra as in Fig. 2 are shown in Fig. 3 after the Doppler corrections appropriate for the PLF motion. Transitions from Ca ($A=46-43$) and Ti ($A=50-46$) are clearly visible, but they show a sizable Doppler broadening at higher energies which is due to the finite size of the Ge detectors. At the same time the TLF γ transitions are smeared out by these corrections and are not seen.

The intensities of γ rays from PLF and TLF gradually decrease with increased E_{loss}. They are not seen at all for the deep inelastic region. The reasons are as follows. Increased E_{loss} results in the evaporation of many neutrons and light charged particles so that the intensity of any particular exit channel decreases. More importantly, however, evaporated neutrons scatter on the Ge detectors, their Compton suppressors, and the NaI detectors of the spin spectrometer producing significant background. Most of the events for large E_{loss} were triggered by 511 keV and γ rays from (n,n'γ) scattering on ^{23}Na, ^{27}Al, ^{72,74}Ge, and ^{127}I. Some of that background can be seen in Fig. 2. Consequently, the present method of identifying discrete transitions can be applied only to the quasielastic region for moderate E_{loss} at the present incident energy or perhaps to more channels and larger E_{loss} for lower bombarding energies.

The subsequent data treatment focusses on the evaporation of neutrons, but the subject of a contribution from charged-particle evaporation and preequilibrium-neutron emission has to be discussed. Since we gated on particular Z of the PLF, any channels resulting from charged-particle evaporation would be visible in the γ ray spectra of the TLF (Fig. 2). As can be seen in Fig. 2(a), ^{150}Nd and ^{149}Pm or ^{150}Pm are observed, in addition to Sm, resulting from 2p and p evaporation, respectively. However, these channels are of weaker intensity compared to the Sm isotopes. No channels resulting from charged-particle evaporation are seen in the Nd system [Fig. 2(b)]. The charged-particle evaporation does not interfere with our results not only because it is small, but also because we consciously gate on γ transitions from neutron-evaporation channels only.

Pre-equilibrium-neutron emission has been studied in detail before.[31–35] Considering the deep inelastic reactions, $\sim$9% of the neutrons were due to preequilibrium emission in the 16 MeV/nucleon ^{12}C + ^{158}Gd reaction and essentially no preequilibrium neutrons were observed in the 12 MeV/nucleon ^{20}Ne + ^{150}Nd reaction.[35] Considering that evidence and the moderate excitation of our system ($E^*_{tot} \sim 105$ MeV), any possible contribution from the preequilibrium neutrons would be small and was neglected.

The kinetic energy loss E_{loss} and the total excitation energy of the system E^*_{tot} were calculated on an event-by-event basis using an iterative procedure of Sobotka *et al.*[16] from the following equations:

$$E_{\text{loss}}=E_1-(E_3+E_4),\quad E^*_{\text{tot}}=E_{\text{loss}}+Q_{gg}\ , \tag{1}$$

where the indexes 1, 3, and 4 refer to the projectile, PLF, and TLF, respectively. E_4 in Eq. (1) was calculated from two-body kinematics using momentum conservation. For the first iteration E_3(primary) was taken as E_3(measured). The ground state Q value, Q_{gg}, was calculated from the liquid-drop model. Both the two-body kinematics and the Q_{gg} calculation requires an assumption about a primary mass split, and its independence on E_{loss}. The assumed masses used in the calculation are given in the second column of Table I. E^*_{tot} from the first iteration was then used to correct the experimental E_3 for the neutron evaporation. For this purpose E^*_{tot} was assumed to be divided equally between the PLF and TLF. In this way the E^*_3 was obtained, then it was corrected for γ emission (deduced from the spin spectrometer results) and divided by S_n+2T (S_n is the neutron separation energy and T is the temperature) to give a PLF mass loss, A_3^{loss}, due to neutron evaporation. The quantity (S_n+2T) was taken as 14 MeV, a reasonable value in this mass range.[36] The initial estimate of E_3 was then improved using the value of A_3^{loss}:

$$E'_3=E_3\frac{A_3}{A_3-A_3^{\text{loss}}}\ , \tag{2}$$

and two additional iterations of the same procedure were made for every event. The calculated values of E^*_{tot} were binned into 6 or 7 energy gates. At the same time the Ge spectra (sum of all Ge) were projected for each gate.

It is necessary to examine how the two assumptions made above (about the fixed primary masses and about the excitation energy division) affected the E_{loss} and E^*_{tot} calculations. The above iterative procedure was repeated by varying the initial masses by as much as four mass units and this changed the E^*_{tot} up to $\sim 6\%$. Similarly, different assumptions about the energy division were applied, which caused deviations in E^*_{tot} increasing approx-

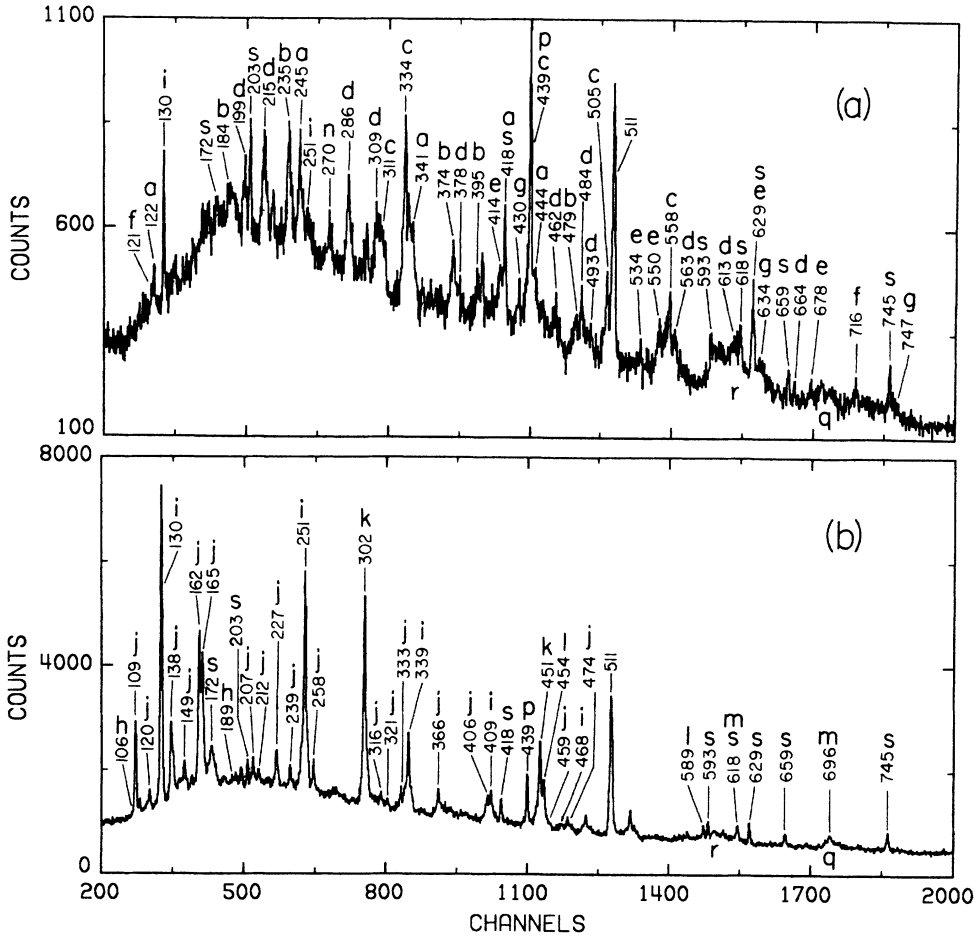

FIG. 2. Combined γ-ray spectra measured with Ge detectors for a 0–120 MeV E^*_{tot} gate. The calibration gain is 0.4 keV/channel. (a) In coincidence with Ca. (b) In coincidence with Ti. Transition assignments are as follows: *a*, ^{152}Sm; *b*, ^{151}Sm; *c*, ^{150}Sm; *d*, ^{149}Sm; *e*, ^{148}Sm; *f*, ^{147}Sm; *g*, ^{146}Sm; *h*, ^{151}Nd; *i*, ^{150}Nd; *j*, ^{149}Nd; *k*, ^{148}Nd; *l*, ^{146}Nd; *m*, ^{144}Nd; *n*, ^{149}Pm or ^{150}Pm; *p*, ^{23}Na; *q*, 691-keV ^{72}Ge; *r*, 596-keV ^{74}Ge; *s*, ^{127}I.

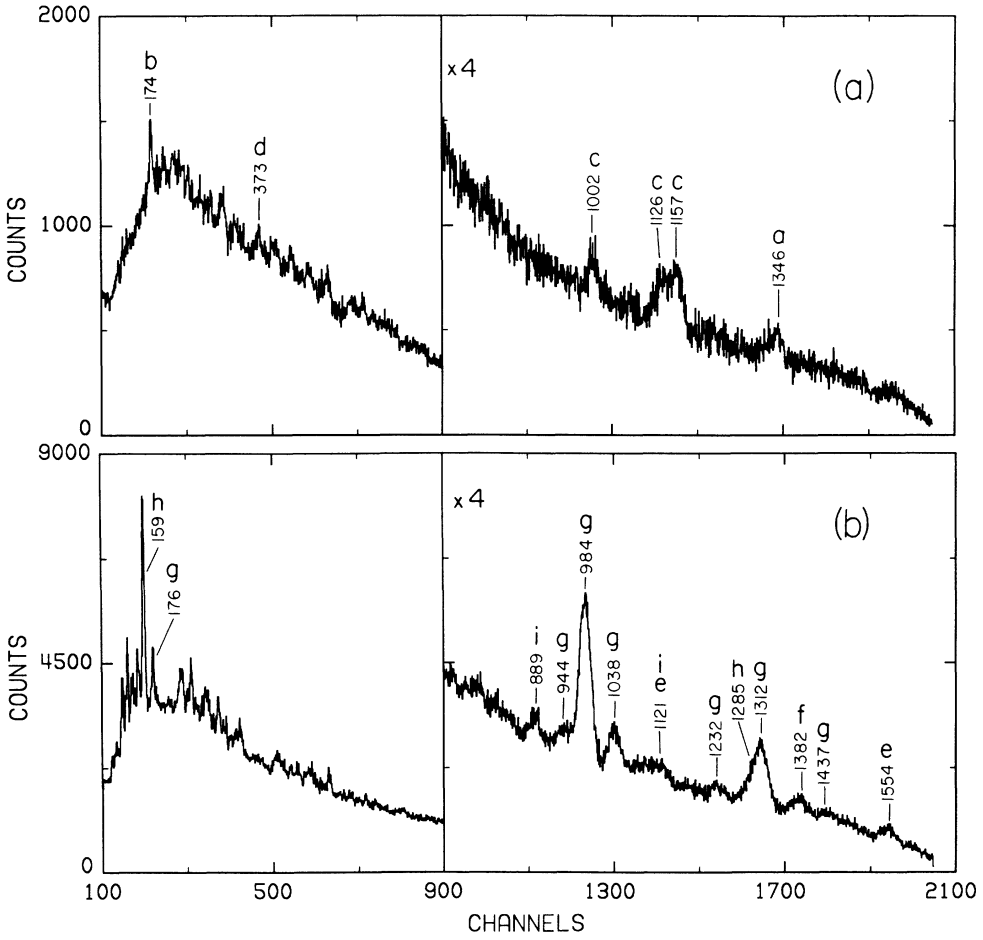

FIG. 3. Combined γ-ray spectra measured with Ge detectors for a 0–120 MeV E^*_{tot} gate and corrected for the Doppler shifts resulting from the PLF motion. The calibration gain is 0.8 keV/channel. (a) In coincidence with Ca. (b) In coincidence with Ti. Transition assignments are as follows: *a*, ^{46}Ca; *b*, ^{45}Ca; *c*, ^{44}Ca; *d*, ^{43}Ca; *e*, ^{50}Ti; *f*, ^{49}Ti; *g*, ^{48}Ti; *h*, ^{47}Ti; *i*, ^{46}Ti.

imately linearly with E^*_{tot} and reaching $\sim 10\%$ at the highest values of E^*_{tot} studied. However, since the E^*_{tot} gates were wide, the E^*_{tot} *centroids* in the gates almost did not change. Consequently, even if the primary masses had been slightly different than assumed in Table I, or had slightly shifted with E_{loss}, or the excitation energy division had been different than equal, that would have not affected our deduced E^*_{tot} centroids significantly.

The γ-ray intensities of the peaks in the Ge spectra were used to determine the mass distributions of Ca, Sm, Ti, and Nd isotopes corresponding to different E^*_{tot} gates. Most of the even-even isotopes were identified by their $2^+ \rightarrow 0^+$ transitions. In the case of the odd-A isotopes the intensities of the peaks feeding the ground state were added, if separate peaks were observed. If only the strongest peak feeding the ground state was observed, its intensity was corrected for the unobserved peaks using the known level schemes. ^{147,145}Nd were not observed. The efficiency calibration of the Ge was done with ^{152}Eu and ^{182}Ta sources using transition intensities from Ref. 37. The γ intensities are plotted in Fig. 4 for the Ca and Sm, and in Fig. 5 for the Ti and Nd isotopes for different E^*_{tot} gates. The uncertainties of the γ intensities (not shown in Figs. 4 and 5 for clarity), including errors due to peak fitting and Ge efficiency vary from $\sim 6\%$ for high intensities to $\sim 25\%$ for the lowest. The mass distributions in Figs. 4 and 5 correspond to secondary products. The average mass numbers (centroids) were calculated for these distributions and the E^*_{tot} is plotted versus the average mass number in Fig. 6 as squares. The vertical bars in Fig. 6 represent the widths of E^*_{tot} gates. The errors of the average mass numbers represent the error of the mean.

TABLE I. Values of average primary mass splits between PLF and TLF (in mass-number units).

Split PLF/TLF	Used to calculate E^*_{tot}	Experimental	Calculated from charge equilibration principle (Ref. 16)
Ca/Sm	47.1/150.9	46.3/151.6[a]	47.1/150.9
Ti/Nd	49.0/149.0	48.5/149.5[a]	52.0/146.0

[a]The uncertainty of mass split is estimated to ± 0.2 mass-number unit for each fragment.

IV. DISCUSSION

Based on the available information we would like to answer the questions of the distribution of primary masses of the two fragments and of the excitation energy division. This must be done with the following constraints: the average primary masses of PLF and TLF have to add up to the mass of the composite system, i.e., $A=198$, and the E^*_{PLF} and E^*_{TLF} have to add up to the experimental E^*_{tot}. Thus, studying the excitation of both PLF and TLF offers a certain degree of consistency.

Figure 6 shows that the average mass number of the secondary products decreases with increasing E^*_{tot}. This is caused by evaporation of neutrons if the primary mass split is independent of E^*_{tot} (or E_{loss}), or it may be caused in part by a change of the primary masses with E_{loss}, The average primary masses at zero excitation were deduced from Fig. 6 as follows. In the case of Ca and Sm the linear least-squares fits were made independently to the first four points in Figs. 6(a) and (b). The fits are not shown in Fig. 6. These fits intercepted the x axes at the values given in the third column of Table I. The sum of the intercepts is equal to 197.9 ± 0.3, so that the mass constraint is satisfied. In the case of Ti and Nd, the thin lines going through the experimental points were extrapolated to zero excitation energy in such a way that the sum of their intercepts with the x axes is equal to 198. The intercepts represent the average primary masses at zero excitation for particular charge splits.

In order to determine the energy division it is necessary to examine how the primary masses may change with E_{loss} (at higher excitations). The experimental primary masses from Table I can be compared with the masses obtained from minimizing the potential energy of two liquid drops in contact with each other (charge equilibrated masses[16]) given in the last column of Table I. The $Z=20$ exit channel will be discussed first. It is seen from Table I that for Ca, the experimental primary mass of 46.3 ± 0.2 is 0.8 unit less than the charge equilibrated value. This small difference may be due to the shell effects in Ca. The similarity between experimental

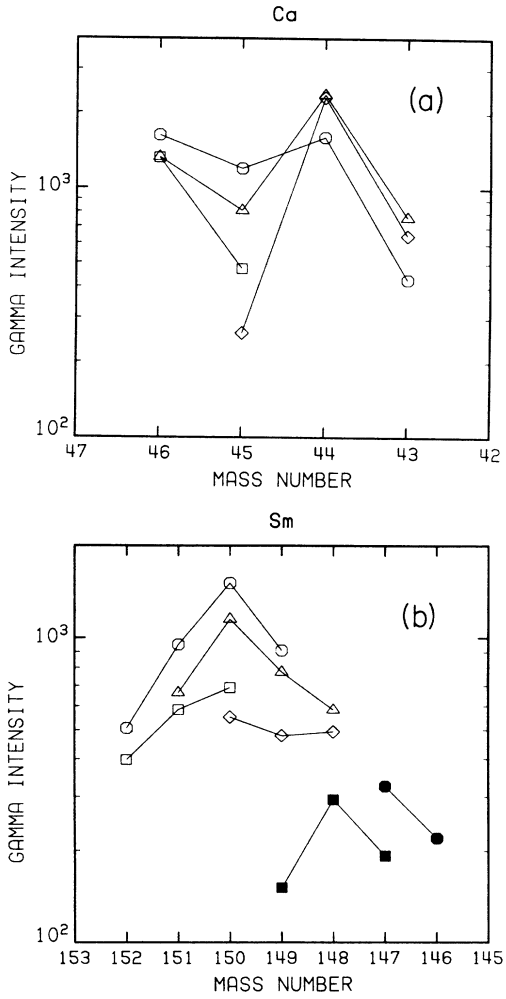

FIG. 4. Secondary mass distributions of (a) Ca and (b) Sm isotopes deduced from intensities of the γ transitions. The E^*_{tot} gates are defined as follows: □, 0–25 MeV; ○, 25–40 MeV; △, 40–55 MeV; ◇, 55–70 meV; ■, 70–90 MeV; ●, 90–120 MeV.

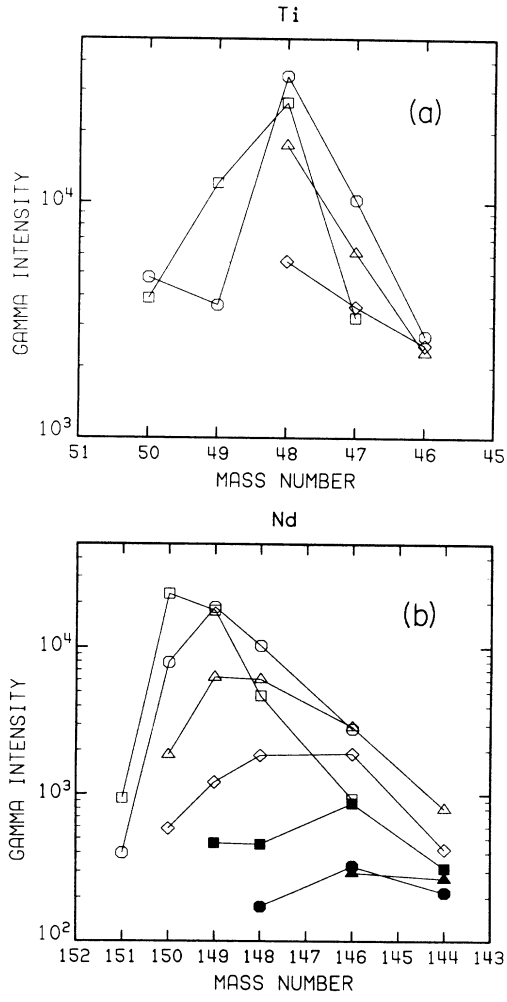

FIG. 5. Secondary mass distributions of (a) Ti and (b) Nd isotopes deduced from intensities of the γ transitions. The E^*_{tot} gates are defined as follows: □, 0–10 MeV; ○, 10–25 MeV; △, 25–40 MeV; ◇, 40–55 MeV; ■, 55–70 MeV; ●, 70–90 MeV; ▲, 90–120 MeV.

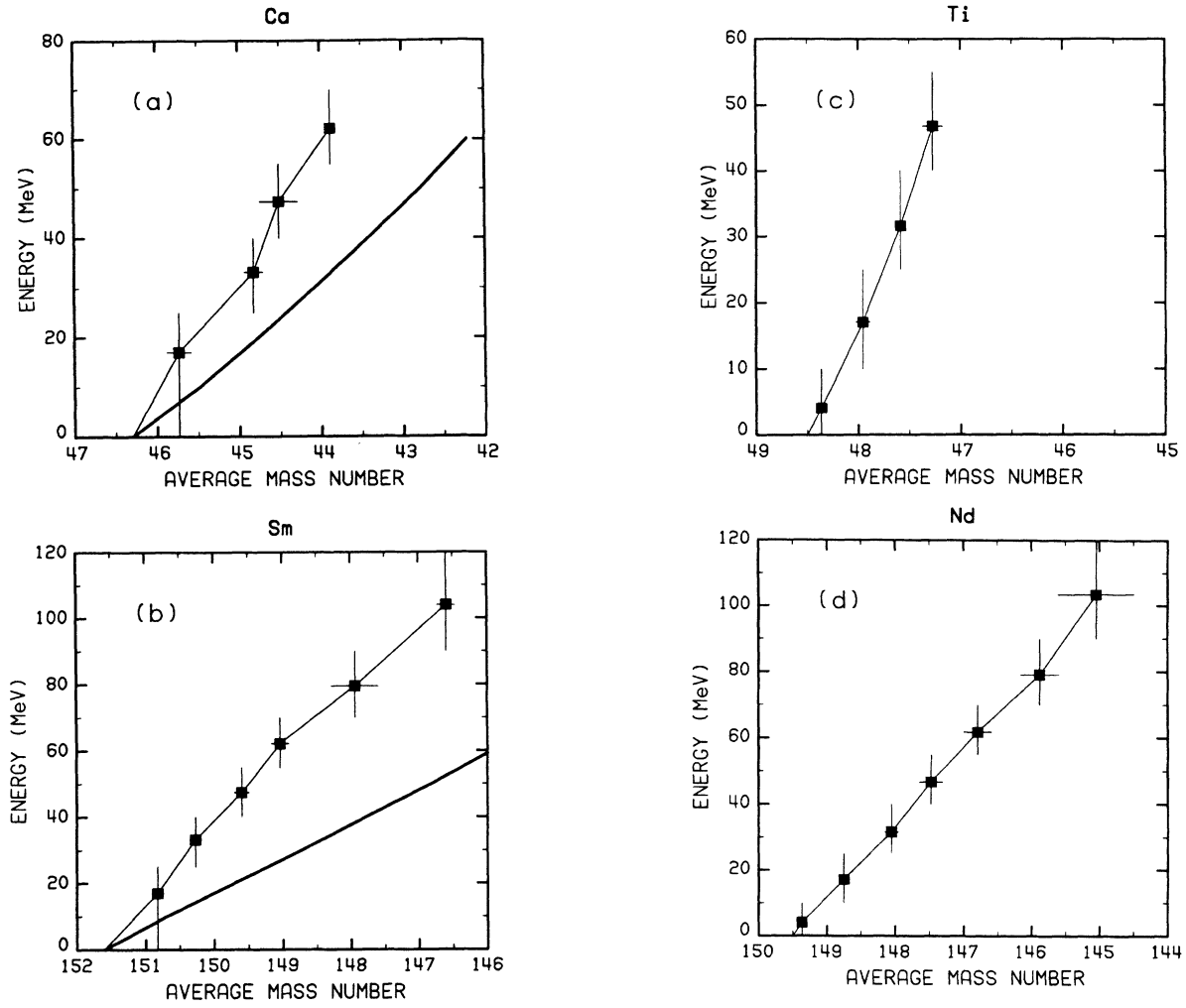

FIG. 6. Excitation energy plotted vs average mass number (secondary) for (a) Ca, (b) Sm, (c) Ti, and (d) Nd isotopes. The points represent the mean values of experimental E^*_{tot}. The vertical bars represent the sizes of E^*_{tot} gates. The heavy solid curves correspond to the statistical-model calculations.

average primary masses of Ca/Sm and the charge equilibrated masses indicates that the mass-to-charge equilibration may occur quickly for this exit channel, even for the low values of E_{loss}. One would not expect the primary mass split to be much different from the charge equilibration prediction for high E_{loss}, because the fragments would have even more time to equilibrate the N/Z degree of freedom. Consequently, we assume for the purpose of further discussion that the average primary mass split between Ca and Sm does not depend significantly on the E_{loss}.

The subject of mass-to-charge equilibration was reviewed by Schröder and Huizenga.[38] For example, a fast equilibration was deduced from the reactions $^{64}Ni + {}^{40}Ca$ and $^{58}Ni + {}^{40}Ar$, with relaxation time of the order of 10^{-22} s. Similar observations were made for the $^{32}S + {}^{238}U$ and $^{86}Kr + {}^{92}Mo$ systems. Other systems like $^{56}Fe + {}^{136}Xe$ and $^{56}Fe + {}^{165}Ho$ did not reveal such a fast charge equilibration.

In order to determine the excitation energy division for the Ca/Sm channel the evaporation of neutrons was simulated with the statistical-model code, PACE.[39] The calculations were done at excitation energy intervals of 10 MeV. The spin distributions used in the calculations were deduced from the fold distributions as measured with the spin spectrometer. Each calculation yielded a distribution of evaporation products. The average mass number of the products was calculated similarly as for the experimental distributions. The statistical model predicts some charged-particle evaporation. However, we take care to select only neutron-evaporation channels from the statistical calculation in order to be comparable with the experimental data. The calculations were done for integral primary masses $^{46,47}Ca$ and $^{151,152}Sm$, which bracket the experimental intercepts in Figs. 6(a) and (b). Then the weighted averages were performed between the neighboring masses, so that the theoretical curves begin from the experimental intercept masses. The theoretical curves are shown as the heavy solid curves in Figs. 6(a) and (b). It was possible to make these averages because the slopes of the theoretical curves for a particular Z are approximately constant for any reasonable choice of the

TABLE II. Ratios of fragment excitation energy to the total excitation energy.

E^*_{tot} (MeV)	E^*_{Ca}/E^*_{tot}	E^*_{Sm}/E^*_{tot}
17	0.41±0.22	0.50±0.23
32	0.59±0.11	0.42±0.08
47	0.51±0.08	0.44±0.06
62	0.53±0.06	0.43±0.04
79		0.48±0.04
104		0.50±0.05

statistical-model parameters. In other words, the whole curve moves to the right for lighter primary mass and to the left for heavier, maintaining its slope approximately constant. This reflects the near constant cost of neutron emission within a reasonable range of mass numbers. At very low excitations the calculated curves had some discontinuities due to the thresholds for neutron evaporation arising from the fixed excitation energies supplied to the statistical calculations. These small discontinuities were smoothed over in Figs. 6(a) and (b).

Using the previous assumption that the average primary masses are approximately constant for the $Z=20$ channel, we can deduce the excitation energy sharing by calculating the ratios of E^*(fragment) from the statistical calculation to the experimental E^*_{tot}. The calculated energies were taken from the heavy solid lines in Figs. 6(a) and (b). The ratios are given in Table II. The errors in Table II were calculated from the second moments of E^*_{tot} distributions in the appropriate gates, and from the uncertainties of intercept masses obtained from Table I. It is seen that for the Ca and Sm complementary fragments, most of the ratios are close to 0.5, indicating an approximately equal energy division, and add up approximately to 1 (within the quoted errors). This offers a consistency check in the analysis. The ratios for Sm at $E^*_{tot}=32$, 47, and 62 MeV are consistently lower than 0.5, but the corresponding Ca ratios are not sufficiently high (except 0.59 at 32 MeV) to allow for different conclusions. For an energy division different from equal, the average mass numbers in Figs. 6(a) and (b) would shift to different values due to neutron evaporation from primary fragments of different excitation. Since E^*_{tot} is the same, the slopes of the experimental lines in Figs. 6(a) and (b) would change in opposite directions for the Ca and Sm fragments. Consequently, the ratios of the unchanged theoretical curves to the experimental ones would yield the appropriate energy division. One should also indicate that if the charge equilibrated masses from Table I were strictly assumed, the fraction of the total excitation energy contained in the Sm fragment would drop from 0.50±0.05 to 0.43±0.04 at the highest E^*_{tot} studied (105 MeV). The two values overlap each other within the quoted errors. The experimental points in Fig. 6 extend to $E_{loss}\sim 105$ MeV for Sm corresponding to 36% kinetic energy damping (100% damping corresponds to purely Coulomb barrier repulsion). The experimental points reach only ~ 62 MeV for Ca. This is caused by the loss of observable intensity of the γ transitions from the PLF due to the Doppler broadening effects.

The nucleon-exchange models predict the excitation energy to be divided nearly equally for a small E_{loss} and a transition toward equilibrium sharing when the energy relaxation increases.[23–26] This prediction is made for the integrated cross sections of the reaction. Our result, while measured for specific exit channel, remains in qualitative agreement with the nucleon-exchange models. In the $Z=20$ exit channel from this investigation net 2p are transferred to the TLF. The approximately equal energy division may suggest, however, that there are more nucleons transferred in both directions washing out the donor/acceptor picture based on the net number of nucleons transferred. A strongly nonequilibrium energy distribution throughout the quasielastic region in the $Z=20$ exit channel is consistent with $^{56}Fe+{}^{165}Ho$ data,[11,22] which show that energy equilibration may occur in the region close to a full damping of kinetic energy.

The situation is different for the $Z=22$ exit channel. One finds from Table I that the average primary mass of Ti at low excitation is 48.5±0.2. Obviously the inelastic scattering dominates here, but there is also on the average 0.5 neutron transfer to the PLF. This primary mass is 3.5 units smaller than that from the charge equilibration (equal to 52, see Table I). The reason for this difference may be due to the fact that there was not enough time for the nuclear mass-to-charge equilibration in this peripheral collision, at least for the lowest E_{loss}. As a result, the primary mass split is dependent on E_{loss}. As discussed before, the system is expected to drift toward the charge equilibration for higher E_{loss} but it is difficult to determine from this data how fast. That would result in neutron transfer from Nd to Ti. Consequently, we cannot use the statistical-model calculations (at fixed masses) to deduce the excitation energy sharing for this exit channel. However, a comparison between the $Z=20$ and 22 exit channels shows that the mass-to-charge equilibration is channel dependent.

ACKNOWLEDGMENTS

The authors wish to acknowledge L. G. Sobotka for valuable discussions and for supplying computer routines. N. Nicolis and L. A. Adler are acknowledged for helpful discussions. Thanks are due to O. El-Ghazzawy for supplying the scanning and plotting computer packages. This work was supported in part by the Division of Nuclear Physics of the U.S. Department of Energy under Contract No. DE-AS02-76ER04052 with Washington University. Oak Ridge National Laboratory is operated by Martin Marietta energy Systems Inc. under Contract No. DE-AC05-840R21400 with the U.S. Department of Energy.

*Deceased.

†Permanent address: Physics Division, Institute of Atomic Energy, Beijing, People's Republic of China.

[1]J. Randrup, Nucl. Phys. **A447**, 133c (1985).

[2]R. G. Stokstad, Lawrence Berkeley Laboratory Report LBL-21580, 1986.

[3]B. Cauvin *et al.*, Nucl. Phys. **A301**, 511 (1978).

[4]C. R. Gould *et al.*, Z. Phys. A **284**, 353 (1978).

[5]B. Tamain *et al.*, Nucl. Phys. **A330**, 253 (1979).

[6]D. Hilscher *et al.*, Phys. Rev. C **20**, 576 (1979).

[7]Y. Eyal *et al.*, Phys. Rev. C **21**, 1377 (1980).

[8]F. Plasil *et al.*, Phys. Rev. Lett. **40**, 1164 (1978).

[9]J. R. Huizenga, W. U. Schröder, J. R. Birkelund, and W. W. Wilcke, Nucl. Phys. **A387**, 257c (1982).

[10]T. C. Awes *et al.*, Phys. Rev. Lett. **52**, 251 (1984).

[11]J. L. Wile, W. U. Schröder, J. R. Huizenga, and D. Hilscher, Phys. Rev. C **35**, 1608 (1987).

[12]R. Vandenbosch *et al.*, Phys. Rev. Lett. **52**, 1964 (1984).

[13]G. Beier *et al.*, Gesellschaft für Schwerionenforschung mBH Scientific Report 1985, 1986, p. 65.

[14]H. Sohlbach *et al.*, Phys. Lett. **153B**, 386 (1985).

[15]M. C. Mermaz *et al.*, Z. Phys. A **324**, 217 (1986).

[16]L. G. Sobotka *et al.*, Phys. Lett. **175B**, 27 (1986).

[17]K. Siwek-Wilczyńska *et al.*, Phys. Rev. C **32**, 1450 (1985).

[18]A. Ray *et al.*, Phys. Rev. Lett. **57**, 815 (1986).

[19]K. Siwek-Wilczyńska *et al.*, Phys. Rev. C **35**, 1316 (1987).

[20]H. R. Schmidt *et al.*, Phys. Lett. **180B**, 9 (1986).

[21]C. P. M. van Engelen, E. A. Bakkum, R. J. Meijer, and R. Kamermans, Nucl. Phys. **A457**, 375 (1986).

[22]D. R. Benton *et al.*, Phys. Lett. **185B**, 326 (1987).

[23]J. Randrup, Nucl. Phys. **A383**, 468 (1982).

[24]H. Feldmeier and H. Spangenberger, Nucl. Phys. **A428**, 223c (1984).

[25]S. K. Samaddar, J. N. De, and K. Krishan, Phys. Rev. C **31**, 1053 (1985).

[26]L. G. Moretto, Z. Phys. A **310**, 61 (1983).

[27]P. J. Siemens, J. P. Bondorf, D. H. E. Gross, and F. Dickmann, Phys. Lett. **36B**, 24 (1971).

[28]M. Jääskeläinen *et al.*, Nucl. Instr. Methods **204**, 385 (1983).

[29]T. K. Alexander and J. S. Forster, in *Advances in Nuclear Physics,* edited by M. Baranger and E. Vogt (Plenum, New York, 1978), Vol. 10, p. 197.

[30]O. Häusser, D. Pelte, T. K. Alexander, and H. C. Evans, Can. J. Phys. **47**, 1065 (1969).

[31]L. Westerberg *et al.*, Phys. Rev. C **18**, 796 (1978).

[32]K. Geffroy Young *et al.*, Phys. Rev. C **23**, 2479 (1981).

[33]E. Holub *et al.*, Phys. Rev. C **28**, 252 (1983).

[34]E. Holub *et al.*, Phys. Rev. C **33**, 143 (1986).

[35]G. A. Petitt *et al.*, Phys. Rev. C **32**, 1572 (1985).

[36]A. H. Wapstra and G. Audi, Nucl. Phys. **A432**, 55 (1985).

[37]R. A. Meyer, Lawrence Livermore Laboratory Report M-100, 1978.

[38]W. V. Schröder and J. R. Huizenga, University of Rochester Report UR-NSRL-281, 1983, Chap. 3.4.

[39]A. Gavron, Phys. Rev. C **21**, 230 (1980).